ACS APPLIED MATERIALS & INTERFACES

Research Article

www.acsami.org

Single Nanowire Electrode Electrochemistry of Silicon Anode by in Situ Atomic Force Microscopy: Solid Electrolyte Interphase Growth and Mechanical Properties

Xing-Rui Liu,[†,‡] Xin Deng,[†] Ran-Ran Liu,[†,‡] Hui-Juan Yan,[†] Yu-Guo Guo,[†] Dong Wang,*[,†] and Li-Jun Wan*[,†]

[†]CAS Key Laboratory of Molecular Nanostructure and Nanotechnology, Beijing National Laboratory for Molecular Sciences, Institute of Chemistry, the Chinese Academy of Sciences, Beijing, 100190, People's Republic of China

[‡]University of Chinese Academy of Sciences, Beijing, 100049, People's Republic of China

Supporting Information

ABSTRACT: Silicon nanowires (SiNWs) have attracted great attention as promising anode materials for lithium ion batteries (LIBs) on account of their high capacity and improved cyclability compared with bulk silicon. The interface behavior, especially the solid electrolyte interphase (SEI), plays a significant role in the performance and stability of the electrodes. We report herein an in situ single nanowire atomic force microscopy (AFM) method to investigate the interface electrochemistry of silicon nanowire (SiNW) electrode. The morphology and Young's modulus of the individual SiNW anode surface during the SEI growth were quantitatively tracked. Three distinct stages of the SEI formation on the SiNW anode were observed. On the basis of the potential-dependent morphology and Young's modulus evolution of SEI, a mixture-packing structural model was proposed for the SEI film on SiNW anode.

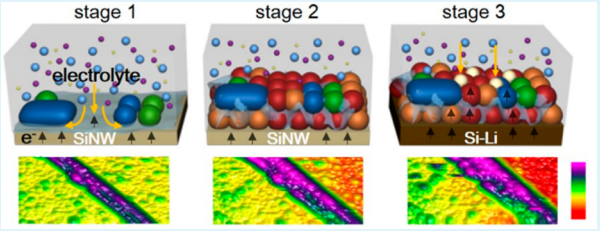

KEYWORDS: *single Si nanowire anode, solid electrolyte interphase (SEI), in situ atomic force microscopy (AFM), Li-ion battery*

INTRODUCTION

The great interest in applying lithium ion batteries (LIBs) to power electric vehicles has induced the research of the anode and cathode materials with higher energy density, extended cycle life, and low cost.[1,2] As for anode materials, silicon is expected to be a potential candidate for its relatively low discharge potential, abundance in crust, and the extremely high theoretical energy capacity (4200 mAh·g^{-1} for $Li_{4.4}Si$),[3] which is almost ten times higher than that of the current graphite anode (372 mAh·g^{-1} for LiC_6).[4] However, the practical application of silicon anode is restricted by its excessive volume variation (nearly 300%) during Li ions insertion and extraction, which leads to mechanical degradation of the electrodes during cycling.[5−7] A number of studies have suggested that nanoscale silicon is more robust than bulk materials with regard to cyclic degradation.[8,9] Among various kinds of silicon nanomaterials, silicon nanowires (SiNWs) have been demonstrated to be capable of withstanding massive volume changes without pulverization, benefiting from their unique 1D nanostructure and enabling them to be promising anodes for LIBs.[10−12]

The solid electrolyte interphase (SEI), forming at the electrode surface mainly during the first cycle, plays a crucial role in anode electrochemistry of LIBs and is closely related to the irreversible capacity loss, conductibility, passivation, and stability of the electrodes.[13] Extensive results have confirmed that the main components of SEI include lithium alkyl carbonate, polyoxyethylene, lithium alkyloxide, Li_2CO_3, and other inorganic compounds.[14,15] An ideal SEI acts like a smart guard, who allows Li ions to pass through but blocks electrons.[16] In the case of silicon anodes, the considerable volume expansion and contraction pose a challenge for stabilizing the SEI on them. The volume change of the silicon could cause SEI collapse and continuous formation during cycling, resulting in electrolyte consumption and capacity loss.[17] Therefore, a flexible and stable SEI is required to protect the electrode from further reaction with the electrolyte and promise long-term cyclic performance. Understanding the formation and the mechanical properties of SEI could provide valuable information about the stability and degradation of the electrodes and is helpful to build effective SEI film for the electrodes with complex structure.

Advanced surface and interface characterization techniques have been applied to understand the formation and properties of SEI. Ex situ approaches often require removing the samples from the electrochemical cells and rinsing traces of the electrolyte with solvents, which may result in mechanical damage or chemical composition changes of the original SEI. Besides, most of the components of SEI are highly sensitive to contamination, air, and humidity. In situ approaches, in contrast, are highly desirable to characterize the nature of SEI

Received: August 28, 2014
Accepted: November 7, 2014
Published: November 7, 2014

directly.[18] Complemented to spectroscopy and electron microscope techniques,[19−24] in situ atomic force microscopy (AFM) has the advantage of monitoring the interface topography and properties simultaneously with nanoscale resolution. Previously, in situ AFM combined with electrochemical control has been applied to the morphological investigation of SEI film or volume effect of silicon film and other bulk electrodes.[25−27] However, the volume effect and interface properties are highly dependent to the dimension scale of the materials. It is of great interest to carry out in situ characterization on electrode materials with a dimension close to that used in a practical battery system, such as nanowire electrodes, which unfortunately has not been reported yet.

In this work, we use individual single crystalline SiNW as a model electrode and focus on the evolution of SEI film and the electrode volume expansion/contraction during the first discharging/charging cycle via in situ AFM. A facile method to prepare single nanowire electrode for in situ AFM characterization is established. The morphological evolution and mechanical properties of the SiNW interface are obtained, and a mixture-packing structural model is proposed for the SEI film on SiNW. This is the first time, to the best of our knowledge, for the interface process and properties of the SiNW anode to be quantitatively identified by in situ AFM. Moreover, the present work demonstrates that the Young's modulus mapping of the electrode interface could provide valuable information about the structure and property of SEI film, which is important for optimizing the electrodes structure and battery systems.

EXPERIMENTAL SECTION

Fabrication of Silicon Nanowires. Silicon nanowires were prepared from an n-type Si(100) wafer with resistivity of 0.05−0.2 Ω·cm by metal assisted electroless etching.[28] In brief, the Si wafers were cleaned by ultrasonication in acetone and ethanol for 10 min, respectively, followed by degreasing in boiling mixed solution of H_2SO_4 and H_2O_2 (98% H_2SO_4/30% H_2O_2 = 7:3 by volume) for 30 min and rinsing with Milli-Q water. Finally, the cleaned Si wafers were dipped in 5% HF solution to remove the native oxides and then immediately immersed in a Teflon beaker that holds an aqueous etchant solution containing 6 mol·L^{-1} HF and 0.04 mol·L^{-1} $AgNO_3$ for 30 min at room temperature. After the etching process, the obtained samples were washed in nitric acid (HNO_3, 37.5%) for 10 min to remove Ag films from the SiNW surfaces. The morphology of fabricated SiNWs was characterized with field-emission scanning electron microscopy (SEM, JEOL 6701F, 5 kV). The structure characterization was performed by field-emission transmission electron microscopy (TEM, JEOL 2011F, 200 kV).

Cyclic Voltammetry Measurement. Cyclic voltammetry (CV) of the SiNWs electrodes was measured in electrochemical half cells with Li metal foil as the counter electrodes. The SiNWs were dispersed on Cu foils as cathodes without any conductive additives and binders. One molar $LiPF_6$ (battery grade, ≥99.99%, Sigma-Aldrich) dissolved in propylene carbonate (PC) (anhydrous, 99.7%, Sigma-Aldrich) served as the electrolyte. A CV test was carried out with an AutoLab (PGSTAT302N, Metrohm) at 0.5 mV·s^{-1} between 1.8 and 0.01 V. All potentials are reported referring to Li/Li^+.

Preparation of Single Silicon Nanowire Electrode. The fabricated SiNWs were ultrasonically dispersed in ethanol and then dropped at a 1.2 × 1.2 cm^2 Si wafer with a 300 nm thick Cu film, which was prepared by magnetron sputtering (PVD75, Kurt J. Lesker). The electrical contact between the SiNW and Cu film was achieved by depositing a carbon film at one end of the SiNW utilizing focused ion beam (FIB) (Helios 600 NanoLab, FEI).

In Situ Single Silicon Nanowire AFM. In situ AFM experiments were conducted with a commercial AFM (Bruker Multimode 8 with a Nanoscope V controller) in a homemade argon-filled glovebox at room temperature. The sample was placed at the bottom of a custom-designed AFM fluid cell with an O-ring to prevent electrolyte leakage. In order to realize in situ electrochemical measurement during morphology and Young's modulus mapping, we combined an external AutoLab with the AFM electrochemical cell to control the potentials. The used electrolyte was 1 mol·L^{-1} $LiPF_6$/PC. All AFM images were acquired in peak force tapping (PFT) mode.

A "scraping" experiment was conducted to remove the SEI in contact mode. The applied scanning force during scraping was slightly larger than that for imaging in contact mode. Then, an in situ quantitative nanomechanics (QNM) experiment was performed in a larger area containing the scraped region to compare and analyze the property of the underlayer and outlayer of the SEI film.

X-ray Photoelectron Spectroscopy Characterization. XPS measurements were performed on an ESCALab220i-XL electron spectrometer (VG Scientific) using 300W Al Kα radiation ($h\nu$ = 1486.6 eV). The base pressure was about 3 × 10^{-9} mbar, and the binding energies were referenced to the hydrocarbon C_{1s} peak at 284.8 eV. The SiNWs electrodes were assembled into electrochemical half cells as described earlier and discharged to 0.6 and 0.01 V and charged to 0.6 V in the first cycle. Then, the samples were removed from the cells in the argon-filled glovebox and rinsed in dimethylcarbonate (DMC) to remove the residual salt and solvent. All samples were dried under vacuum and then transported to the XPS facility in sealed bags.

RESULTS AND DISCUSSION

Single SiNW Electrode Preparation. The SEM images of as-prepared SiNWs fabricated on n-type Si(100) substrate are shown in Figure 1a. The straight SiNWs are always

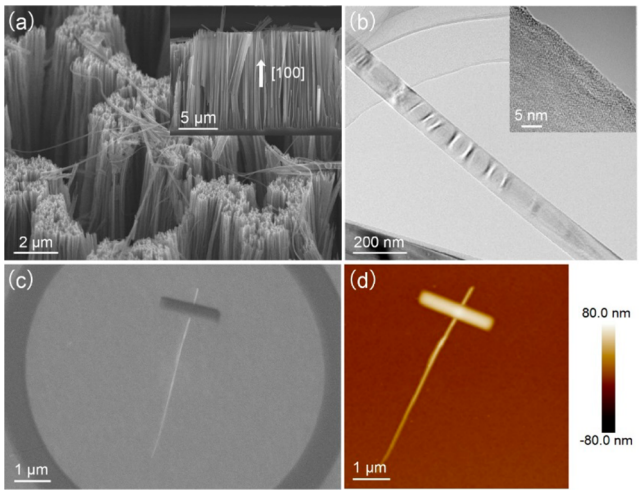

Figure 1. (a) SEM image of SiNWs arrays fabricated on a Si(100) wafer with the inset of a side-view SEM image of the SiNWs. (b) TEM and high-resolution TEM (inset) images of a SiNW with the orientation of [100]. (c) SEM image and (d) AFM image of the same single SiNW anode fixed on the Cu film substrate.

perpendicular to the etched surface and orient in the [100] directions, as shown in the side-view SEM image (inset).[29] The length of the SiNWs is ca. 12 μm, and their diameter sizes vary from a few tens to hundreds of nanometers. Figure 1b shows the TEM images of a single silicon nanowire. The high-resolution TEM image (inset) confirms that the SiNW is single crystalline.

The single silicon nanowire anode is fabricated by fixing a SiNW on a 300 nm thick Cu film supported by a Si wafer. A tape-like carbon pad is deposited on the SiNW by FIB. Bonding the nanowire to the Cu film not only avoids nanowire electrode

floating in the electrolyte but also ensures good electrical contact between the nanowire and Cu film. Figure 1c,d shows the SEM and AFM images of a single SiNW anode. A carbon circle is deposited around the anode and serves as a marker for finding the SiNW under the optical microscope easily. The single silicon nanowire model anode is able to react with the electrolyte thoroughly for its nanoscale dimension. Thus, we can monitor the SEI evolution on SiNW at distinct discharge and charge states, which is difficult to achieve for bulk or collective electrode materials.

Electrochemical Measurement. Figure 2 shows the cyclic voltammogram of SiNWs electrodes between 1.8 and 0.01 V in

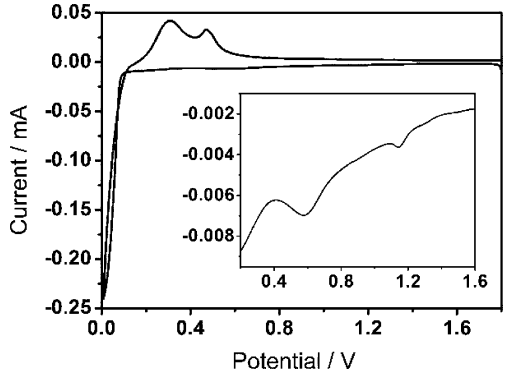

Figure 2. First cyclic voltammogram of the SiNWs anodes in 1 mol·L^{-1} $LiPF_6$/PC at a scan rate of 0.5 mV·s^{-1}. The inset shows the onset of current flow above 0.2 V.

1 M $LiPF_6$/PC. Two small cathodic peaks are observed at ca. 1.14 and 0.58 V, respectively (inset in Figure 2), which disappear in the subsequent cycles (Supporting Information Figure S1). Hence, the above two peaks can be attributed to the reduction reactions of electrolyte and are closely related to the SEI formation. Moreover, the absence of corresponding anodic peaks means that the decomposition of electrolyte is irreversible. A sharp increase of cathodic current at potentials below 0.1 V can be assigned primarily to the intercalation of Li ions. The two anodic peaks appear at 0.31 and 0.47 V, respectively, corresponding to the extraction of Li ions from the SiNWs. To sum up, the CV results suggest that the SEI formation mainly takes place in the first discharge/charge cycle and the Li ions can be inserted/extracted reversibly in pure PC-based electrolyte.[30,31]

In Situ AFM Observation of SEI Growth. The surface morphology evolution of the single SiNW anode during the first cycle was followed by the peak force tapping (PFT) mode using in situ AFM. PFT mode can effectively minimize the damage of the sample surface during scanning for its unique operating mode.[32] The primary SEI film or its upper layer is so gentle and sticky that it may be removed during AFM scanning by contact or even tapping mode.[33] PFT mode operates at even lower forces than tapping mode so that can keep SEI from erosion by the tip during AFM imaging.

Figure 3a–g presents the in situ AFM images of a SiNW anode (see the SEM image in Supporting Information Figure S2) during the first discharging process. In Figure 3a, some particle-like precipitates are observed on the SiNW surface, presumably corresponding to the decomposition of electrolyte on the surface above 1.1 V. When the potential is decreased to 0.4 V, no significant morphological changes can be seen on the SiNW surface except for a few inconspicuous new granules.

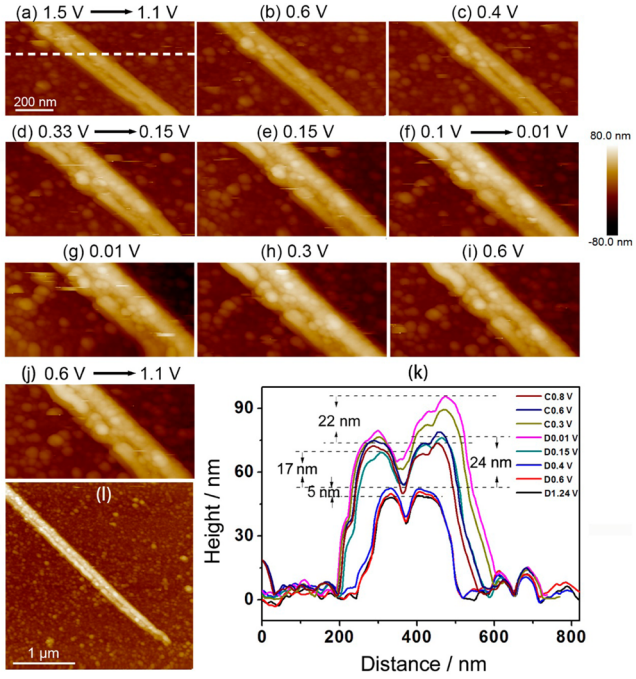

Figure 3. (a–j) The in situ AFM height images of a single SiNW anode during the first cycle at different discharge/charge states. The scan direction is from bottom to top, and the scan area is 1 × 0.5 μm^2. (k) Cross-section analysis of the height of the location marked by a white dashed line during the cycle. (l) The AFM image of the SiNW after the first cycle.

When the potential is further reduced to less than 0.33 V, a rough and inhomogeneous layer of particle-like deposition almost covers the whole nanowire. During the discharge process, we notice that the height and lateral dimension of the film increase significantly, although most particles on the SiNW surface do not change much. At potentials below 0.1 V, the SiNW swells evidently, primarily due to the intercalation of Li ions. Besides, several new particles deposit randomly on the surface shown in Figure 3f,g, indicating new SEI growth. This result suggests that the formation of SEI is not completed at potentials above lithiation but rather occurs by accompanying the Li ions insertion below 0.1 V.[34]

The evolution of the total height of SiNW and SEI was quantitatively examined by the cross-section analysis in Figure 3k. There is a slight increase of height and width (~5 nm) from 1.2 to 0.4 V, corresponding to the growth of the primary SEI with respect to the cathode reaction process of the small current peaks around 1.14 and 0.58 V. In contrast, the primary SEI is much thinner than that which forms from a higher potential in EC-based electrolyte solution.[27] When the SiNW is discharged to 0.15 V, the height rapidly increases by 17–24 nm, mainly attributed to the growth of SEI. After Li ions intercalation, the height of SiNW increases to more than 90 nm. However, the thickness of the newly formed SEI could not be quantified, as volume expansion of bulk SiNW during the lithiation process contributes to the height increase as well.

On the basis of the morphological analysis, the formation of SEI on SiNW goes through three stages with distinct features under different potentials: (i) above 0.4 V, the SEI grows slowly and the primary SEI is thin (ca. 5 nm). Only a few particles exist on the SiNW, and the granular coverage is about 30%. (ii) Rapid growth of the SEI occurs below 0.33 V with a thicker and grainy feature. The coverage of the SEI film at 0.15 V is almost

100%. (iii) During the lithiation process below 0.1 V, the SEI keeps growing with a slower rate than the second stage. New particles appear on the SiNW surface during this process. As a result, the SiNW anode is completely covered by a SEI film with an estimated thickness of ca.22−29 nm after the formation process.

Since AFM cannot directly analyze the components of SEI, we carried out XPS as a complementary method to get the chemical information on the SEI. The XPS results suggest that the SEI formed on SiNW in 1 M $LiPF_6$/PC is mainly composed of organic species, LiF, Li_2CO_3, and/or other carbonates. LiF is primarily formed at the first growth stage of SEI, and Li_2CO_3 is mainly formed at lower potentials (see the details in Supporting Information Figure S3).

Next, we have observed the morphology evolution of SiNW in the charging process as shown in Figure 3h−j. The height of SiNW gradually decreases upon delithiation for Li ions extraction from SiNW. However, no dramatic morphological changes of the SEI surface could be recognized. In a wide scan (3×3 μm^2) after the first cycle shown in Figure 3l, the structure of SiNW remains intact and no cracks can be observed (see the in situ AFM images of this scan area in Supporting Information Figure S4). The result supports that SiNWs have the advantage of bearing volume changes during the first lithiation/delithiation cycle, in comparison to Si thin film and amorphous Si nanorods which do not.[22,26] Furthermore, during the process of volume expansion and contraction, the SEI maintains a sound condition without cracks or being scraped off, indicating that a stable SEI film can form on the SiNW anode in the $LiPF_6$/PC system. Moreover, the SEI remains stable during the second cycle, and the SiNW exhibits good performance while enduring the huge volume changes (see the details in Supporting Information Figure S5).

It should be noted from Figure 3k that there is an obvious difference on the height changes between the left and the right parts of the SiNW anode during the volume expansion and contraction process. A bigger height and lateral dimension change appears on the right part. As previously mentioned, the structure of the SiNW anode used in the experiment has a single crystal nature and its orientation is [100]. The outer surfaces around SiNW are with different crystallographic planes. It seems that the volume expansion of crystal SiNW is orientation dependent. This result is consistent with recent findings of anisotropic swelling in lithiation of Si nanopillars and SiNWs based on SEM and TEM studies.[35,36]

Young's Modulus of SEI. Mechanical properties of SEI are of great importance for the long-term cyclic performance of LIBs electrode materials especially for the high capacity anode materials with large volume changes. Here, we utilize peak force quantitative nanomechanics (PF-QNM), an extended application of the PFT mode,[37,38] to measure the Young's modulus of the SiNW surface during SEI growth. The working principle and calibration process of QNM are described in the Supporting Information.

The in situ Young's modulus mapping was obtained simultaneously when capturing the morphology of SiNW. As shown in Figure 4a, the Young's modulus of the SiNW surface is nearly 700 MPa at the beginning of discharge (1.5 V). As the potential drops to 0.6 V, the Young's modulus reduces to around 150 MPa. The decrease in the modulus results from a thin primary SEI film formed on the surface of SiNW anode upon discharge shown in Figure 3b,k. When the potential is swept to 0.4 V, the Young's modulus remains almost

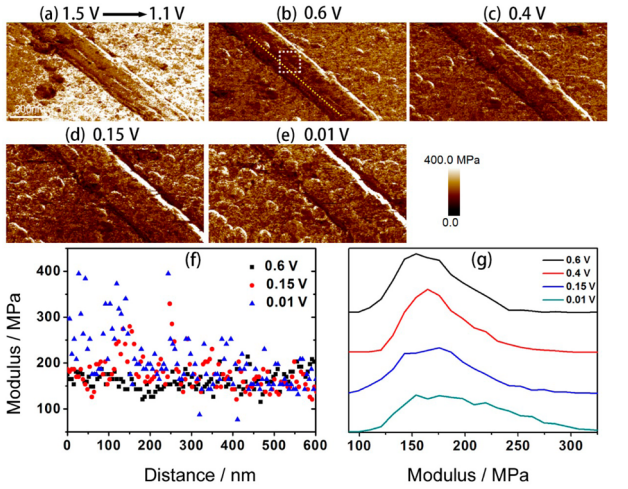

Figure 4. (a−e) The AFM images of Young's modulus mapping of a single SiNW anode in the first discharge process. The scan direction is from bottom to top, and the scan area is 1×0.5 μm^2. (f) The distribution of Young's modulus along the location marked with a dashed yellow line. (g) The statistic values of Young's modulus of the area marked with a dashed white box.

unchanged. At the same time, no significant changes can be observed from the morphology (Figure 3c). After the second growth stage of SEI, as shown in Figure 4d, the Young's modulus increases slightly and becomes inhomogeneous at 0.15 V, which is attributed to the growth of a thick and particle-like SEI on the nanowire. When the potential is further reduced to 0.01 V, the modulus becomes more inhomogeneous as shown in Figure 4e. On the basis of the above results, the inhomogeneity and magnitude of the modulus of the SiNW surface are found to present an ascending trend during discharging process.

In order to clarify the distribution and trend of the modulus during SEI growth, we analyze the Young's modulus of the location marked by a dashed yellow line along the SiNW in the discharging process. According to Figure 4f, the modulus becomes more inhomogeneous and increases obviously during the SEI growth. Furthermore, statistical analysis of the distribution of the modulus for the same sites on SiNW is carried out as shown in Figure 4g. A slightly increasing trend of the statistic mean value and distribution of modulus with the growth of the SEI film is observed. The Young's modulus results indicate that the structure and components of SEI dynamically change during the formation progress, which is consistent with the XPS analysis.

SEI Structure and Thickness. In order to analyze the cross-section profile and thickness of the SEI film, a "scraping" experiment was conducted. Figure 5a shows the height image of the scraped area. Several grains can be seen on the surface of the scraped SiNW, suggesting that residual SEI is left on the anode surface. The SiNW is verified to be structurally sound with no cracks and impairment after scraping the SEI off. Figure 5b displays the corresponding image of Young's modulus mapping. It is clear that the Young's modulus of the surface of the scraped SiNW (marked with A and B) is slightly smaller than that of the outer surface of the intact SEI (marked with C). Figure 5c,d displays the cross-section analysis of the height and Young's modulus of the SEI on SiNW. In Figure 5c, the Young's modulus value of the intact SEI surface is around 250 MPa, while the modulus of the scraped area is around 200 MPa,

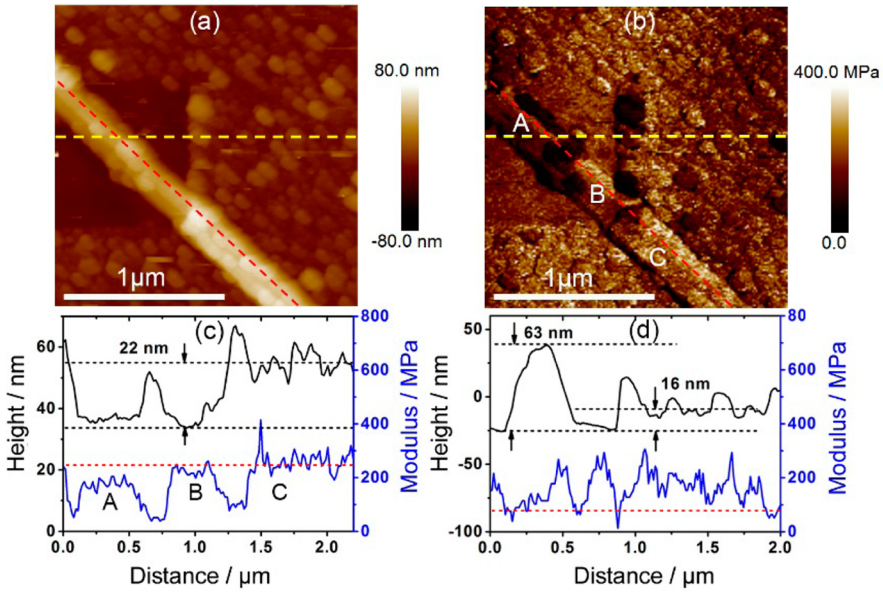

Figure 5. Images of height (a) and modulus (b) of the SiNW anode after being scraped. The line profiles of the topography (black) and modulus (blue) along the SiNW (c) (marked with a dashed red line) and along the horizontal cross section (d) (marked with a dashed yellow line).

implying a relatively hard outlayer and a slightly soft underlayer of the SEI film. From the cross-section analysis, we also find that the SEI is rough with uneven thickness along the SiNW.

To further evaluate the thickness of the residual SEI, the applied force during scraping in contact mode was slightly increased. We kept scraping the SiNW until it was broken off, and the last AFM image of the intact nanowire was used for the thickness analysis. We overlaid the AFM images of the same position of a SiNW at different scraping stages to evaluate the depth profile of SEI. Figure 6 presents the line profiles of the

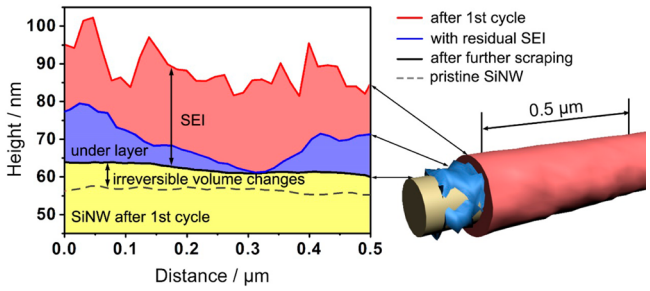

Figure 6. Line profiles along the axis of the SiNW after the first cycle (red line), with residual SEI (blue line), and after further scraping (black line) and pristine SiNW (dashed gray line).

height along the axis of SiNW after the first cycle (red line), with residual SEI (blue line), and after further scraping to remove the SEI (black line) and pristine SiNW (dashed gray line). The SEI is rough on the anode surface with a thickness range of 18−38 nm. The volume of SiNW after the first cycle expands obviously. An irreversible height increase is estimated to be around 14% compared to the pristine SiNW.

A range of research has focused on the structure and formation mechanism of the SEI film for LIBs.[14,39,40] For different battery systems, the composition and structure of SEI is strongly affected by the electrode materials and electrolyte composition. A popular double-layer or multilayer model of the SEI film can be described in brief as a porous organic layer close to electrolyte and a compact inorganic layer next to the electrode.[33,41,42] In contrast, our results show that the surface of SEI has a slightly bigger Young's modulus, and there is no such obvious feature of the layered structure of the SEI film on the SiNW anode in the $LiPF_6$/PC system.

On the basis of the observation results of in situ morphology and Young's modulus evolution of SEI, a model diagram of the growth and structure of SEI is displayed in Figure 7. In the first

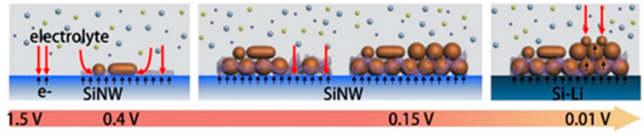

Figure 7. Model diagram of the growth and structure of the SEI on the SiNW anode during the first discharge process.

growth stage above 0.4 V, the electrolyte accepts electrons from the surface of the SiNW to form the primary SEI composed of carbonates, organic compounds, and LiF. The primary SEI film is thin and has low granular coverage. In the second growth stage below 0.33 V, a rough and inhomogeneous film rapidly covers the whole nanowire. The new growth of SEI is close to the surface of the electrode. During this stage, the Young's modulus slightly increases presumably due to more inorganic substances such as Li_2CO_3 being generated. In the third growth stage along with lithiation process, the SEI grows slowly and new particles appear on the SEI surface. This model describes the development of the three growth stages of SEI and accounts for the slightly increasing trend of the distribution and statistic value of Young's modulus. Studies have suggested that the SEI is an accumulation of numerous particles of different chemical compositions with boundaries between them.[39,43] According to our model and in situ observation, the SEI is an accumulation of the inorganics and organics mixture with a slightly hard outer shell. The mixture-packing structure is flexible, stable, and capable of adapting to the volume changes of SiNW.

CONCLUSIONS

In conclusion, we demonstrated the single nanowire in situ AFM method to understand the SEI growth on the SiNW anode. The formation process and mechanical properties of the SEI film on the SiNW anode in 1 M $LiPF_6$/PC were characterized through various operation modes of in situ AFM. Three distinct stages were observed in the formation of SEI at different potentials. A thin primary film formed on the SiNW anode above 0.4 V. When the potential was decreased to 0.33 V, the surface was soon covered by a thick and particle-like SEI. The growth of the SEI continued with the alloying process below 0.1 V. After the first cycle, the SEI formed on the SiNW was rough and inhomogeneous with a thickness of 28 ± 10 nm. The SEI film remained intact after the first cycle, showing the abilities to withstand the big volume change during the first lithiation and delithiation cycle. The Young's modulus of the complete SEI film shows the statistics value within a range of 50−400 MPa, consistent with the composition nature of the SEI. The modulus of the SiNW interface slightly increased with the growth of SEI, indicating the evolution of composition of the film, which was correlated with ex situ XPS analysis. A mixture-packing structure model is proposed for the SEI film on the SiNW anode. Our results show new insights and complexity of the SEI film for the Si anode with different morphology. Finally, we envision that in situ AFM investigation of the single electrode electrochemistry process could be applicable to other electrode systems of LIB.

ASSOCIATED CONTENT

Supporting Information

Cyclic voltammetry curves of SiNWs anode; SEM image of the single SiNW anode prepared for in situ AFM; XPS analysis of the SiNW surface; more in situ AFM images of SiNW electrodes; the calibration procedures in the PF-QNM experiment. This material is available free of charge via the Internet at http://pubs.acs.org.

AUTHOR INFORMATION

Corresponding Authors

*Fax: +86-10-62558934. E-mail: wangd@iccas.ac.cn.
*Fax: +86-10-62558934. E-mail: wanlijun@iccas.ac.cn.

Author Contributions

The manuscript was written through contributions of all authors. All authors have given approval to the final version of the manuscript.

Notes

The authors declare no competing financial interest.

ACKNOWLEDGMENTS

This work was supported by the Ministry of Science and Technology (Grant Nos. 2011YQ03012415, 2011CB932300, and 2011CB808700), National Natural Science Foundation of China (Nos. 21121063, 21127901, and 21373237), and the Chinese Academy of Sciences.

REFERENCES

(1) Dunn, B.; Kamath, H.; Tarascon, J. M. Electrical Energy Storage for the Grid: A Battery of Choices. *Science* **2011**, *334*, 928−935.
(2) Etacheri, V.; Marom, R.; Elazari, R.; Salitra, G.; Aurbach, D. Challenges in the Development of Advanced Li-Ion Batteries: A Review. *Energy Environ. Sci.* **2011**, *4*, 3243−3262.
(3) Boukamp, B.; Lesh, G.; Huggins, R. All-Solid Lithium Electrodes with Mixed-Conductor Matrix. *J. Electrochem. Soc.* **1981**, *128*, 725−729.
(4) Zhang, W.-J. A Review of the Electrochemical Performance of Alloy Anodes for Lithium-Ion Batteries. *J. Power Sources* **2011**, *196*, 13−24.
(5) Pharr, M.; Suo, Z.; Vlassak, J. J. Measurements of the Fracture Energy of Lithiated Silicon Electrodes of Li-Ion Batteries. *Nano Lett.* **2013**, *13*, 5570−5577.
(6) Liu, X. H.; Zhong, L.; Huang, S.; Mao, S. X.; Zhu, T.; Huang, J. Y. Size-Dependent Fracture of Silicon Nanoparticles During Lithiation. *ACS Nano* **2012**, *6*, 1522−1531.
(7) He, Y.; Yu, X.; Li, G.; Wang, R.; Li, H.; Wang, Y.; Gao, H.; Huang, X. Shape Evolution of Patterned Amorphous and Polycrystalline Silicon Microarray Thin Film Electrodes Caused by Lithium Insertion and Extraction. *J. Power Sources* **2012**, *216*, 131−138.
(8) Wu, H.; Cui, Y. Designing Nanostructured Si Anodes for High Energy Lithium Ion Batteries. *Nano Today* **2012**, *7*, 414−429.
(9) Szczech, J. R.; Jin, S. Nanostructured Silicon for High Capacity Lithium Battery Anodes. *Energy Environ. Sci.* **2011**, *4*, 56−72.
(10) Chan, C. K.; Peng, H.; Liu, G.; McIlwrath, K.; Zhang, X. F.; Huggins, R. A.; Cui, Y. High-Performance Lithium Battery Anodes Using Silicon Nanowires. *Nat. Nanotechnol.* **2007**, *3*, 31−35.
(11) Xiao, Y.; Hao, D.; Chen, H.; Gong, Z.; Yang, Y. Economical Synthesis and Promotion of the Electrochemical Performance of Silicon Nanowires as Anode Material in Li-Ion Batteries. *ACS Appl. Mater. Interfaces* **2013**, *5*, 1681−1687.
(12) Chakrapani, V.; Rusli, F.; Filler, M. A.; Kohl, P. A. Silicon Nanowire Anode: Improved Battery Life with Capacity-Limited Cycling. *J. Power Sources* **2012**, *205*, 433−438.
(13) Xu, K. Nonaqueous Liquid Electrolytes for Lithium-Based Rechargeable Batteries. *Chem. Rev.* **2004**, *104*, 4303−4418.
(14) Aurbach, D. Review of Selected Electrode−Solution Interactions Which Determine the Performance of Li and Li Ion Batteries. *J. Power Sources* **2000**, *89*, 206−218.
(15) Verma, P.; Maire, P.; Novák, P. A Review of the Features and Analyses of the Solid Electrolyte Interphase in Li-Ion Batteries. *Electrochim. Acta* **2010**, *55*, 6332−6341.
(16) Lu, P.; Harris, S. J. Lithium Transport within the Solid Electrolyte Interphase. *Electrochem. Commun.* **2011**, *13*, 1035−1037.
(17) Wu, H.; Zheng, G.; Liu, N.; Carney, T. J.; Yang, Y.; Cui, Y. Engineering Empty Space between Si Nanoparticles for Lithium-Ion Battery Anodes. *Nano Lett.* **2012**, *12*, 904−909.
(18) Sazhin, S. V.; Gering, K. L.; Harrup, M. K.; Rollins, H. W. Highly Quantitative Electrochemical Characterization of Non-Aqueous Electrolytes and Solid Electrolyte Interphases. *J. Electrochem. Soc.* **2014**, *161*, A393−A402.
(19) Mukherjee, P.; Lagutchev, A.; Dlott, D. D. In Situ Probing of Solid-Electrolyte Interfaces with Nonlinear Coherent Vibrational Spectroscopy. *J. Electrochem. Soc.* **2012**, *159*, A244−A252.
(20) Stancovski, V.; Badilescu, S. In Situ Raman Spectroscopic−Electrochemical Studies of Lithium-Ion Battery Materials: A Historical Overview. *J. Appl. Electrochem.* **2013**, *44*, 23−43.
(21) Li, J.-T.; Zhou, Z.-Y.; Broadwell, I.; Sun, S.-G. In-Situ Infrared Spectroscopic Studies of Electrochemical Energy Conversion and Storage. *Acc. Chem. Res.* **2012**, *45*, 485−494.
(22) Ghassemi, H.; Au, M.; Chen, N.; Heiden, P. A.; Yassar, R. S. In Situ Electrochemical Lithiation/Delithiation Observation of Individual Amorphous Si Nanorods. *ACS Nano* **2011**, *5*, 7805−7811.
(23) Zeng, Z.; Liang, W. I.; Liao, H. G.; Xin, H. L.; Chu, Y. H.; Zheng, H. Visualization of Electrode-Electrolyte Interfaces in $LiPF_6$/EC/DEC Electrolyte for Lithium Ion Batteries Via in Situ Tem. *Nano Lett.* **2014**, *14*, 1745−1750.
(24) Bridel, J.; Azaïs, T.; Morcrette, M.; Tarascon, J.; Larcher, D. In Situ Observation and Long-Term Reactivity of Si/C/CMC Composites Electrodes for Li-Ion Batteries. *J. Electrochem. Soc.* **2011**, *158*, A750−A759.
(25) Beaulieu, L. Y.; Cumyn, V. K.; Eberman, K. W.; Krause, L. J.; Dahn, J. R. A System for Performing Simultaneous in Situ Atomic

Force Microscopy/Optical Microscopy Measurements on Electrode Materials for Lithium-Ion Batteries. *Rev. Sci. Instrum.* **2001**, *72*, 3313−3319.
(26) Martin, L.; Martinez, H.; Ulldemolins, M.; Pecquenard, B.; Le Cras, F. Evolution of the Si Electrode/Electrolyte Interface in Lithium Batteries Characterized by Xps and Afm Techniques: The Influence of Vinylene Carbonate Additive. *Solid State Ionics* **2012**, *215*, 36−44.
(27) Tokranov, A.; Sheldon, B. W.; Li, C.; Minne, S.; Xiao, X. In Situ Atomic Force Microscopy Study of Initial Solid Electrolyte Interphase Formation on Silicon Electrodes for Li-Ion Batteries. *ACS Appl. Mater. Interfaces* **2014**, *6*, 6672−6686.
(28) To, W.-K.; Tsang, C.-H.; Li, H.-H.; Huang, Z. Fabrication of N-Type Mesoporous Silicon Nanowires by One-Step Etching. *Nano Lett.* **2011**, *11*, 5252−5258.
(29) Chen, C.-Y.; Wu, C.-S.; Chou, C.-J.; Yen, T.-J. Morphological Control of Single-Crystalline Silicon Nanowire Arrays near Room Temperature. *Adv. Mater.* **2008**, *20*, 3811−3815.
(30) Pereira-Nabais, C.; Świątowska, J.; Chagnes, A.; Ozanam, F.; Gohier, A.; Tran-Van, P.; Cojocaru, C.-S.; Cassir, M.; Marcus, P. Interphase Chemistry of Si Electrodes Used as Anodes in Li-Ion Batteries. *Appl. Surf. Sci.* **2013**, *266*, 5−16.
(31) Chen, H.; Xiao, Y.; Wang, L.; Yang, Y. Silicon Nanowires Coated with Copper Layer as Anode Materials for Lithium-Ion Batteries. *J. Power Sources* **2011**, *196*, 6657−6662.
(32) Trtik, P.; Kaufmann, J.; Volz, U. On the Use of Peak-Force Tapping Atomic Force Microscopy for Quantification of the Local Elastic Modulus in Hardened Cement Paste. *Cem. Concr. Res.* **2012**, *42*, 215−221.
(33) Cresce, A. v.; Russell, S. M.; Baker, D. R.; Gaskell, K. J.; Xu, K. In Situ and Quantitative Characterization of Solid Electrolyte Interphases. *Nano Lett.* **2014**, *14*, 1405−1412.
(34) Chan, C. K.; Ruffo, R.; Hong, S. S.; Cui, Y. Surface Chemistry and Morphology of the Solid Electrolyte Interphase on Silicon Nanowire Lithium-Ion Battery Anodes. *J. Power Sources* **2009**, *189*, 1132−1140.
(35) Lee, S. W.; McDowell, M. T.; Choi, J. W.; Cui, Y. Anomalous Shape Changes of Silicon Nanopillars by Electrochemical Lithiation. *Nano Lett.* **2011**, *11*, 3034−3039.
(36) Liu, X. H.; Zheng, H.; Zhong, L.; Huang, S.; Karki, K.; Zhang, L. Q.; Liu, Y.; Kushima, A.; Liang, W. T.; Wang, J. W.; Cho, J.-H.; Epstein, E.; Dayeh, S. A.; Picraux, S. T.; Zhu, T.; Li, J.; Sullivan, J. P.; Cumings, J.; Wang, C.; Mao, S. X.; Ye, Z. Z.; Zhang, S.; Huang, J. Y. Anisotropic Swelling and Fracture of Silicon Nanowires During Lithiation. *Nano Lett.* **2011**, *11*, 3312−3318.
(37) Adamcik, J.; Berquand, A.; Mezzenga, R. Single-Step Direct Measurement of Amyloid Fibrils Stiffness by Peak Force Quantitative Nanomechanical Atomic Force Microscopy. *Appl. Phys. Lett.* **2011**, *98*, 193701.
(38) Adamcik, J.; Lara, C.; Usov, I.; Jeong, J. S.; Ruggeri, F. S.; Dietler, G.; Lashuel, H. A.; Hamley, I. W.; Mezzenga, R. Measurement of Intrinsic Properties of Amyloid Fibrils by the Peak Force QNM Method. *Nanoscale* **2012**, *4*, 4426−4429.
(39) Peled, E.; Golodnitsky, D.; Ardel, G. Advanced Model for Solid Electrolyte Interphase Electrodes in Liquid and Polymer Electrolytes. *J. Electrochem. Soc.* **1997**, *144*, L208−L210.
(40) Winter, M. The Solid Electrolyte Interphase-the Most Important and the Least Understood Solid Electrolyte in Rechargeable Li Batteries. *Z. Phys. Chem.* **2009**, *223*, 1395−1406.
(41) Lu, P.; Li, C.; Schneider, E. W.; Harris, S. J. Chemistry, Impedance, and Morphology Evolution in Solid Electrolyte Interphase Films During Formation in Lithium Ion Batteries. *J. Phys. Chem. C* **2014**, *118*, 896−903.
(42) Shi, S.; Lu, P.; Liu, Z.; Qi, Y.; Hector, L. G.; Li, H.; Harris, S. J. Direct Calculation of Li-Ion Transport in the Solid Electrolyte Interphase. *J. Am. Chem. Soc.* **2012**, *134*, 15476−15487.
(43) Christensen, J.; Newman, J. A Mathematical Model for the Lithium-Ion Negative Electrode Solid Electrolyte Interphase. *J. Electrochem. Soc.* **2004**, *151*, A1977−A1988.